Sensors & Actuators: B. Chemical 441 (2025) 138000

Contents lists available at ScienceDirect

Sensors and Actuators: B. Chemical

journal homepage: www.elsevier.com/locate/snb

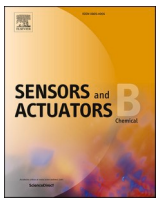

Integration of AC bias-stabilized SiNRFETs with microscale Ag/AgCl pseudo-reference electrodes for lab-on-chip biosensing application

Zheqiang Xu [a], Yingtao Yu [a], Paul Solomon [b], Zhen Zhang [a,*]

[a] Ångström Laboratory, Division of Solid-State Electronics, Department of Electrical Engineering, Uppsala University, Uppsala SE-75121, Sweden
[b] IBM Thomas J. Watson Research Center, Yorktown Heights, NY 10598, USA

ARTICLE INFO

Keywords:
AgCl/Ag pseudo-reference electrode
On-chip integration
Ion-sensitive field-effect transistors
Microfluidics
Drift
AC pulse gate bias

ABSTRACT

Ion-sensitive field-effect transistors (ISFETs) are highly promising for lab-on-chip integration due to their excellent scalability, high sensitivity, and rapid response times. However, on-chip integration of reliable microscale reference electrodes, essential for ISFET operation in microfluidic systems, remains a significant challenge. This study presents a microfluidic pH meter that integrates silicon nanoribbon field-effect transistor (SiNRFET) sensors with on-chip microscale AgCl/Ag pseudo-reference electrodes (p-REs). The microscale p-REs, fabricated using CMOS-compatible processes and protected with a photoresist layer, demonstrated rapid stabilization and long-term stability. Moreover, the short distance between the integrated p-REs and the paired SiNRFET sensors within the microfluidic environment minimized streaming potential, ensuring measurement accuracy regardless of flow rate variations. In addition, applying an AC pulse gate bias effectively reduced ISFET signal drift caused by ion penetration into the pH-sensitive layer, enhancing the system's reliability for long-term monitoring. To showcase the platform's biosensing capabilities, the microfluidic pH meter was finally used to monitor bacterial metabolism on-chip via measuring pH changes induced by metabolic activity with microliter-level samples. This work establishes a robust lab-on-chip biosensing platform, enabling real-time and long-term biosensing in microscale environments.

1. Introduction

Lab-on-chip integration of bio/chem-sensors with microfluidics offers numerous advantages, such as short response time [1,2], small sample volume [3–5], and high analysis throughput [6]. Among the sensor technologies available, ion-sensitive field-effect transistors (ISFETs) are particularly well-suited for lab-on-chip applications due to their size scalability [7] for large-scale integration [8–10], high sensitivity and selectivity [11–13], and compatibility with automated systems [14]. ISFET operation relies on a reference electrode (RE) to define the liquid potential, allowing surface potential changes induced by the specific adsorption of target ions on the sensor surface to effectively shift the threshold voltage (ΔV_{th}), thereby modulating the ISFET's channel current [15]. However, downsizing REs to match the microscale dimensions of microfluidic systems remains a critical challenge [15–17].

The challenge in miniaturizing RE lies in downscaling the volume of the filling electrolyte [16–20]. One practical approach to realize on-chip REs is to integrate pseudo-reference electrodes (p-REs) on the surface of the sensor chip, without the need of filling electrolytes [21]. AgCl/Ag p-RE is one of the most used p-REs owing to its simple structure and non-polarizable characteristics [22]. Although the potential of AgCl/Ag p-RE could be affected by concentration variations of halide ions in the solution, AgCl/Ag p-RE is still a good choice for monitoring samples with a constant halide concentration (such as blood, urine [23], bacteria culture [24], etc). The most reported method for fabricating on-chip p-REs is screen-printing [17,18,22]. However, screen-printed AgCl/Ag electrodes typically have lateral pattern sizes exceeding 100 μm [25–27] and thicknesses over 20 μm [28–31], which limits their compatibility with microfluidic designs featuring arrays of microscale chambers for sample compartmentalization and analysis [32–36]. Ideally, a microscale RE and an ISFET sensor need to be integrated into each discrete chamber, with a dimension less than 100 μm, to enable parallel analysis of samples with small volume [37–39]. Another method with size scalability to fabricate AgCl/Ag p-REs is to utilize CMOS-compatible metal deposition and patterning techniques to form Ag electrodes on the ISFET chips, then use chemical treatment to form a AgCl layer on the Ag electrodes [5,40].

In addition to the integration process, the long-term stability of an

* Corresponding author.
E-mail address: zhen.zhang@angstrom.uu.se (Z. Zhang).

https://doi.org/10.1016/j.snb.2025.138000
Received 29 January 2025; Received in revised form 14 May 2025; Accepted 18 May 2025
Available online 20 May 2025

integrated lab-on-chip system is crucial for its real applications, especially for continuous monitoring of samples. Welch et al. [41] demonstrated a repeatable drift pattern in ISFETs by periodically cycling the gate bias between operational and zero-bias states. Jamasb et al. [42] reported a post data-processing method to correct the drift in ISFET. However, this method is mainly applicable when pH changes rates far exceed drift rates. Thorough validation, particularly concerning both the p-RE stability and ISFET signal drift within the microfluidic environment, is essential for their real applications.

In this work, we fabricated microscale (5 μm in lateral dimension) AgCl/Ag p-REs together with silicon nanoribbon field-effect transistors (SiNRFETs) on the same sensor chip using fully CMOS-compatible process technology. The sensor chip was further integrated with microchannels to realize a microfluidic pH meter. We found that covering the microscale p-REs with a porous photoresist protection layer could effectively prevent the failure of p-REs. With the photoresist protection, the on-chip AgCl/Ag p-RE demonstrated rapid stabilization and excellent long-term stability. Compared to published studies, our on-chip AgCl/Ag p-RE is the first to achieve a size below 10 μm while maintaining good long-term stability [43–46]. Furthermore, the short distance between the integrated AgCl/Ag p-RE and the pairing SiNRFET also ensured a negligible impact from the streaming potential to the measurement accuracy. The integrated microfluidic pH meter could operate in both static and flow modes with fast and close-to-Nernstian responses. In addition, the signal drift induced by the ion penetration into the pH sensing layer in the SiNRFET sensors was also investigated. We demonstrated that using an AC pulse gating bias could well mitigate the ion penetration problem, thus minimizing the ISFET signal drift. Finally, we utilized the microfluidic pH meter to monitor the metabolic activity of bacteria in the microchannel. Using ISFET to monitor cellular metabolism via measuring metabolic-activity-induced pH changes in the culturing media was a novel approach developed in our lab [24]. Utilizing a microfluidic channel will significantly reduce the amount of sample required for the test. This demonstration highlights the potential of the integrated system for on-chip analysis of cell samples, including quantifying cell density and real-time monitoring of cellular metabolic responses to various stimuli, such as drug treatments.

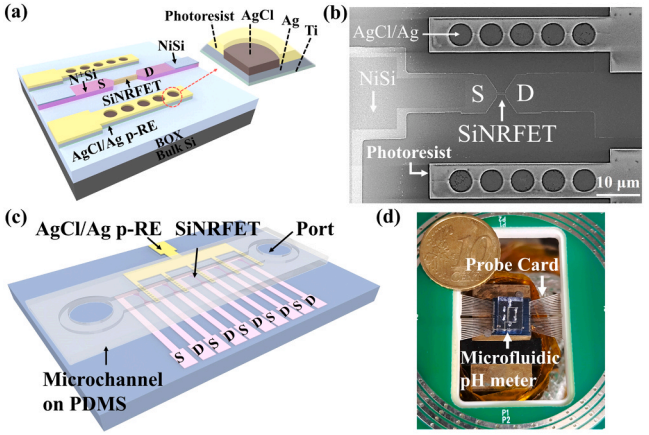

Fig. 1. The microfluidic pH meter integrated with SiNRFETs, AgCl/Ag p-REs, and microfluidics. (a) The 3D schematic of the SiNRFET sensor and AgCl/Ag p-REs on a sensor chip. (b) Top-view SEM image of the SiNRFET sensor and AgCl/Ag p-REs. (c) The 3D schematic of the microfluidic pH meter, with a PDMS microchannel integrated on the sensor chip. (d) Image of the microfluidic pH meter connected to a probe card.

2. Experimental section

2.1. SiNRFET sensors and microscale p-REs fabrication

A three-dimensional (3D) schematic of a sensor chip with a SiNRFET sensor and microscale AgCl/Ag p-REs is shown in Fig. 1(a). The device was fabricated on a (100) silicon-on-insulator (SOI) wafer with a 55-nm-thick lightly doped (N_a=1 ×10^{15} cm^{-3}) *p*-type Si layer on top of a 145-nm-thick SiO_2 (BOX) layer, using standard Si process technology. The SiNRFET channel was patterned in the lightly doped *p*-type SOI layer with 600 nm in length and 500 nm in width, using electron beam lithography (EBL) followed by a reactive ion etching process.

The source (S) and drain (D) terminals of the FET were heavily implanted by arsenic (As) to reach 1 × 10^{20} cm^{-3} *n*-type doping. To further reduce the contact resistance to S/D, a 5-nm-thick Nickel (Ni) layer was deposited on the S/D via lift-off, and subsequently annealed at 400 °C in N_2 for 30 s using a rapid thermal process (RTP) to form NiSi. Afterward, a 4-nm-thick HfO_2 passivation layer was deposited on the whole chip surface by atomic layer deposition (ALD) at 170 °C. It also served as the pH sensing layer for pH measurements. Finally, the sensor chip was annealed in forming gas (5 % H_2 in N_2) at 400 °C for 30 min to passivate the channel/gate oxide interface traps. A more detailed fabrication process of the Si ISFET sensors can be found in our previous work [24,47].

For p-REs integration, 150 nm thick and 5 μm wide comb-like Ag electrodes (see Fig. S1) with a 5 nm thick Ti adhesion layer underneath were evaporated on the HfO_2 layer, using a metal evaporation and lift-off process. The Ag electrodes were covered by photoresist (UVN 2300–0.5) with 5 contact holes (5 μm in diameter, beside the SiNRFET) opened through the photoresist layer, via an EBL process, to expose the Ag electrodes underneath, as illustrated in Fig. 1(a). The exposed Ag electrodes were further treated with a $FeCl_3$ solution (0.1 M) for 1 min at 20 °C to form a AgCl layer at the exposed surface of Ag. The completed AgCl/Ag p-REs and a SiNRFET sensor were shown in the top-view scanning electron microscope (SEM) image in Fig. 1(b). The cross-section image of the p-RE is shown in Fig. S2. Ag p-REs with the same photoresist coverage but without the $FeCl_3$ solution treatment were fabricated in parallel as control samples.

2.2. Integration of the microfluidic pH meter

The SiNRFET sensor chip was integrated with a microchannel to form a microfluidic pH meter, as shown in Fig. 1(c). The microchannel (20 μm thick and 150 μm wide) was made of polydimethylsiloxane (PDMS; Silgard 184; base/curing agent ratio is 10:1) using a SU8 mold. The PDMS microchannel and the SiNRFET chip were bonded together after surface O_2 plasma activation. A specifical designed X/Y/Z/θ stage is used to align the sensor chip and the microfluidics during the bonding process. The structure details of the microfluidic pH meter can be found in Fig. S1.

2.3. Electrical measurement

The long-term stability of the p-REs was evaluated by measuring the open-circuit potential (OCP) of the p-REs against a commercial AgCl/Ag RE (eDAQ, ET072, filled with 3.4 M KCl solution) in 30 mM KCl solution. OCPs were also measured under varying KCl concentrations and pH levels to evaluate the chloride sensitivity and pH sensitivity of the p-REs. The OCPs were recorded using a B1500 semiconductor device analyzer equipped with four source measurement units (SMUs). Details of the electrical measurement setup is displayed in Fig. S3. Then stable AgCl/Ag p-REs were paired with SiNRFETs in the microfluidic pH meter to characterize the drift in SiNRFETs during pH monitoring. The electrical measurements were conducted using an HP4155A semiconductor parameter analyzer, with the sensor chip being accessed via a probe card, as shown in Fig. 1(d). Four SiNRFETs were measured

simultaneously using a switch unit (Keysight 34970 A). The drain current - I_D was then monitored in real-time with a constant source-drain voltage (V_{DS}) at 0.3 V and a gate voltage (V_G) applied to the AgCl/Ag p-RE. The I_D change was then converted to ΔV_{th} based on the transfer curve (I_D Vs. V_G) of the SiNRFET, with the detailed conversion method described in section S3 of the Supplementary Information. The same setup was also employed to monitor pH changes in the microchannel during on-chip bacterial culture.

2.4. Reagents and solutions

All reagents were of analytical grade or equivalent and were purchased from Sigma-Aldrich unless stated otherwise. All solutions were prepared using deionized water.

For preparing KCl solutions with varying pH values to measure the response of the SiNRFET to pH changes, a 0.1 M KCl solution was first adjusted to pH 3 using 0.1 M hydrochloric acid (HCl), with the pH determined using a calibrated pH meter. The pH 3, 0.1 M KCl solution was sequentially diluted tenfold with a pH 7, 0.1 M KCl solution to obtain 0.1 M KCl solutions with pH values of 4, 5, and 6. The pH values of other solutions mentioned in this study were directly measured using the pH meter (Mettler Toledo, FiveEasy). The same dilution strategy was used to prepare KCl solutions (3 M to 0.003 M) for p-RE chloride response measurement.

2.5. Escherichia coli samples preparation

The Genotype of bacterial strains used in this study is *Escherichia coli* (*E. coli*) K12 MG1655. Bacterial strains were grown in LB at 37 °C shaking at 200 rpm (revolutions per minute). The bacterial concentration of *E. coli* in the overnight culture was determined by measuring the optical density at 600 nm (OD600, Implen Diluphotometer™). After a 10-fold dilution, the OD600 was measured as 0.64, corresponding to a bacterial concentration of 5×10^9 cells/mL in the original overnight culture [48,49]. To prepare *E. coli* solutions with different concentrations for on-chip culture, 100 µL of the overnight culture was centrifuged at 1950 × g (rcf) for 3 min. The supernatant was removed, and the pellet was resuspended in fresh culture medium (LB + 1 wt.% glucose) to obtain samples with the desired bacterial concentrations.

3. Results and discussions

3.1. Characterization of the microscale p-REs

The potential stability of the microscale thin-film AgCl/Ag p-RE was first characterized, and compared to that of the microscale Ag p-REs. The chloride sensitivities of both Ag p-REs and AgCl/Ag p-REs are shown in their OCP results measured against a commercial KCl (3.4 M)/AgCl/Ag RE in KCl solution at 20 °C (see Fig. 2(a)). Both p-REs exhibit near-Nernstian responses to the variation of [Cl^-] (59.5 mV/ (Δlog [Cl^-]) for Ag p-RE and 56 mV/ (Δlog [Cl^-]) for AgCl/Ag p-RE). This confirms that reaction (1) is the potential determination reaction for both Ag p-RE and AgCl/Ag p-RE.

$$AgCl_s + e^- \leftrightarrow Ag_s + Cl^- \quad (1)$$

The OCP plots also show that AgCl/Ag p-REs stabilize much quicker (less than 20 s) than the Ag p-REs (60 min). Substantial initial OCP drift of Ag p-RE and much longer stabilization time may be induced by gradual AgCl formation on the Ag surface after being immersed in the

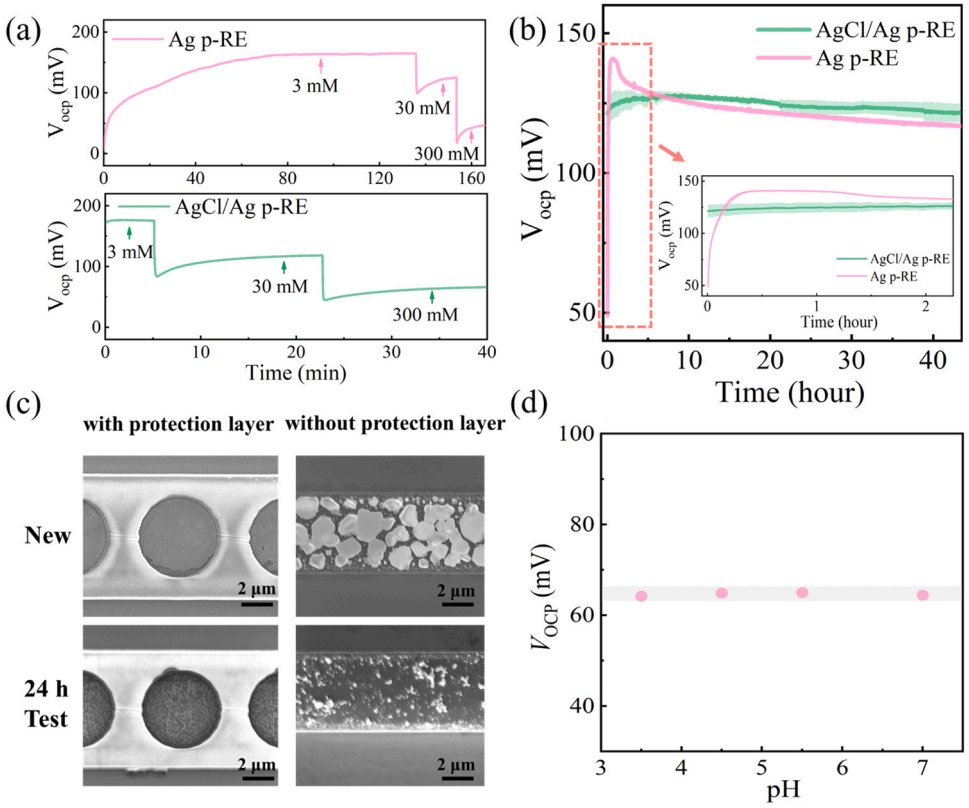

Fig. 2. The OCP measurements for a p-RE (Ag or Ag/AgCl, both with resist protection) vs. a commercial KCl (3.4 M)/AgCl/Ag RE in KCl solution at 20 °C. (a) The OCP results of a Ag p-RE and a AgCl/Ag p-RE, both against the commercial RE with varying Cl^- concentration. (b) The OCP results of a Ag p-RE and a AgCl/Ag p-RE in 30 mM KCl solution at pH 7. The light-shaded areas depict the standard deviations calculated based on the results of 3 OCP tests. (c) Top-view SEM images of a AgCl/Ag p-RE with (left) and without (right) the photoresist protection layer before and after the 24-hour OCP monitoring. (d) The OCP of AgCl/Ag p-RE in 300 mM KCl solution at different pH levels. The gray region represents the standard deviation calculated based on the results of 3 OCP tests.

solution. Therefore, the AgCl/Ag p-REs will be much more reliable than the Ag p-REs, especially for real-time monitoring.

The long-term stability of the p-REs was also recorded over 40 h in a 30 mM KCl solution at pH 7, with data presented in Fig. 2(b). Again, the AgCl/Ag p-RE showed a much quicker stabilization time. After reaching a steady state, both Ag p-RE and AgCl/Ag p-RE showed a stable OCP against the commercial RE over the recorded period. The OCP drift for the Ag p-RE and AgCl/Ag p-RE is 0.4 mV/h and 0.2 mV/h, respectively. The slight OCP drift might be induced by the recrystallization or the slow dissociation of the AgCl layer [22,31], according to the investigation of the morphology change of the AgCl layer before and after the 24-hour tests (see Fig. 2(c_left)). We also tested a AgCl/Ag p-RE without the resist protection, it lost electrical connection after about 30 mins in the tests. This was due to the peeling of the unprotected p-RE under fluid flow, as confirmed by the investigation of the morphology change of the unprotected p-RE shown in Fig. 2(c_right). The photoresist protection could prevent the peeling of the electrode and significantly extend the lifetime of the AgCl/Ag p-RE. Table 1 compares the minimum feature size and stability of various all-solid-state AgCl/Ag electrodes. The on-chip AgCl/Ag p-RE in this work demonstrates smallest minimum feature size while maintaining excellent stability.

In addition, the function of the RE is to fix the liquid potential for pH measurements using ISFETs. An ideal RE should not respond to pH variations. As shown in Fig. 2(d), the OCP of our AgCl/Ag p-RE (against a commercial RE) does not respond to pH variations. This further confirms the reliability of the AgCl/Ag p-REs for pH measurements.

3.2. The microfluidic pH meter based on SiNRFETs and microscale p-REs

The SiNRFET sensor was then characterized with the liquid potential defined by the stable AgCl/Ag p-RE (with photoresist protection) in the microfluidic pH meter. The microfluidic pH meter can operate in either static or flow mode. The liquid samples were delivered into the microfluidic pH meter by syringe pumps. The device characterization was done in 0.1 M KCl solution (pH 6.5) at 20 °C. The I_D-V_{DS} characteristics of the SiNRFET are presented in Fig. S5. A V_{DS} of 0.3 V was applied in all subsequent measurements. The transfer characteristic, I_D vs V_G of SiNRFET was also measured under static mode, as shown in Fig. 3(a).

The SiNRFET has an n-type channel and exhibits a subthreshold swing of 93 mV/dec with an on-to-off current ratio (I_{on}/I_{off}) of ~10^4. Notably, the gate leakage I_G remains below 1 nA. The pH responses of the SiNRFET sensor under both the static and flow modes are shown in Fig. 3(b). A typical current signal from the pH measurements is depicted in Fig. 3(b_upper) (flow mode), in which pH decreasing leads to the rise of I_D. Then, the I_D change was converted to ΔV_{th} using the transfer curve in Fig. 3(a). ΔV_{th} exhibits a Nernstian response with a sensitivity of around 60 mV/pH for both static and flow modes Fig. 3(b_lower).

The long-term stability of the microfluidic pH meter in the flow mode was also compared for the AgCl/Ag p-RE with and without the photoresist protection, as shown in Fig. 3(c). I_D was sampled in 0.1 M KCl solution at pH 6.5 under a 10 μL/min flow rate. For the AgCl/Ag p-RE with the photoresist protection, the I_D shows some initial drift in the first 1.5 h before stabilization (it corresponds to 12 mV ΔV_{th} drift). However, for the AgCl/Ag p-RE without the photoresist protection, I_D started decreasing after the first 30-minute test, and the electrical connection was completely lost after one hour. This is consistent with the cracks forming and peeling of the AgCl/Ag p-RE shown in Fig. 2(c_right). This test also highlights the critical role of photoresist protection over the AgCl/Ag p-REs for the reliability of the integrated microfluidic pH meter.

When an ISFET sensor is used under flow mode, the streaming potential between the RE and the sensor needs to be kept constant to avoid its disturbance to the measured signal [52]. Since the streaming potential is proportional to the distance between the RE and the sensor, as well as the flow rate [53], it is important to keep the RE as close to the sensor as possible to minimize the streaming potential interference to the measurements caused by the flow rate variations. In our microfluidic pH meter, the AgCl/Ag p-RE is only 10 μm away from the paring SiNRFET sensor, as shown in Fig. 1(c). This short distance ensures a negligible impact from the streaming potential to the pH signal, as evidenced by the same pH responses measured by our microfluidic pH meter under both static and flow modes (see Fig. 3(b)). It was further confirmed by measurements under alternating flow rates using an on-chip p-RE and a commercial RE at the microfluidic outlet as shown in Fig. 3(d). The long-distance between the commercial RE and the SiNRFET induces notable streaming potential, causing significant I_D changes with flow rate shifts (purple curve). In contrast, the on-chip AgCl/Ag p-RE minimizes streaming potential effects to the measurement due to its proximity to the SiNRFET (green curve). The streaming potential calculation detailed in section S5 of the Supplementary Information further confirms that variations in flow rate have a negligible influence on the SiNRFET measurement when using the integrated on-chip AgCl/Ag p-RE.

3.3. Minimizing SiNRFET drift by using AC pulse gate bias

Controlling the drift in the ISFET devices is also crucial for their real applications, especially for long-term monitoring [54]. We measured the I_D drift of the SiNRFET sensors, in pH 6.5, 0.1 M KCl solution at 20 °C and static mode, with the device being biased to subthreshold and linear regions via the on-chip AgCl/Ag p-RE and a commercial RE. The I_D drift was then converted to ΔV_{th} as shown in Fig. 4(a). The SiNWFET sensor exhibits a similar level of drift with both types of REs, indicating that the measured drifts originate from the SiNWFET itself. And a stronger V_G bias leads to a larger ΔV_{th} drift.

It was reported that the drift in SiNRFETs could be caused by the penetration of hydrogen ions into the HfO_2 layer under the positive gate bias [55]. Interstitial hydrogen is a common impurity in ALD-grown HfO_2 [56,57], and the interstitial hydrogen in HfO_2 is known to be a negative-U impurity [58,59]. In our SiNRFET measurements, we speculate that H^+ ions migrate to the HfO_2 surface under the electric field generated by the positive gate bias, and then get reduced at the HfO_2/Si channel interface to negatively charged impurities, as illustrated in Fig. 4b_left. This leads to the ΔV_{th} drift towards more positive values. Using an AC pulse gate bias can potentially suppress the drift, since negative gate bias could oxidize the interstitial hydrogen to H^+ ions at the HfO_2/liquid interface, as illustrated in Fig. 4(b).

Table 1
Comparison of stability, minimum feature size and thickness of all-solid-state AgCl/Ag electrodes.

Ref	Fabrication methods	Structure	Minimum feature size	Thickness	Drift (mV/h)
Yiheng [50]	Inkjet-printing	PVC/KCl (liquid) /AgCl/Ag	100 μm	300 nm	0.3
Rebecca [25]	Screen-printing	PVA-KCl /AgCl/Ag	1 mm	200 μm	0.7
Sindre [18]	Screen-printing	AgCl/Ag	5 mm	> 10 μm	0.01
Qiaofeng [20]	Evaporation	PVB/NaCl (liquid) /AgCl/Ag	1 mm	200 nm	1.7
Hyo-Ryoung [51]	Evaporation	Nafion/ AgCl/Ag	1 mm	800 nm	0.1
Jing [43]	Sputtering	AgCl/Ag	150 μm	10 μm	1.5
Dongwon [44]	Lithography & evaporation	AgCl/ Ag	28 μm	2 μm	0.3
This work	Lithography & evaporation	Photoresist /AgCl/Ag	5 μm	150 nm	0.2

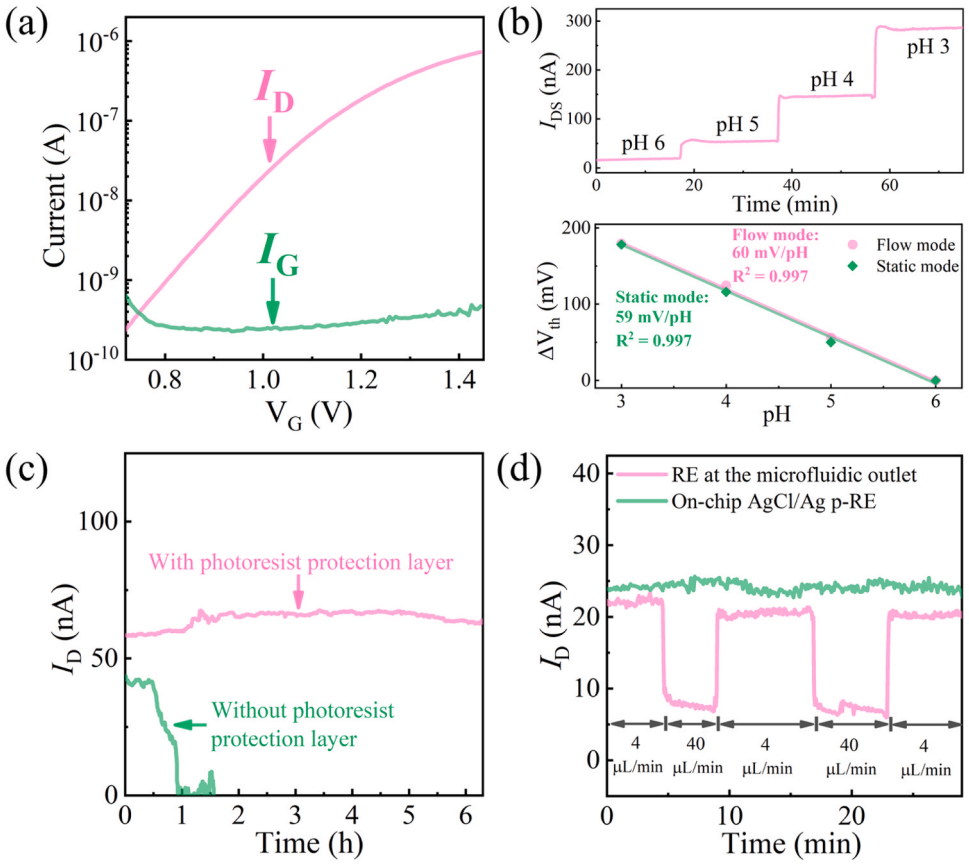

Fig. 3. pH measurements using the microfluidic pH meter at 20 °C. (a) Transfer characteristics (I_D-V_G) at V_{DS} = 0.3 V of the SiNRFET at pH 6.5, 0.1 M KCl (b) pH measurements using the microfluidic pH meter in 0.1 M KCl under flow mode (4 µL/min) (upper), and the comparison of the measured pH responses under flow mode and static mode (lower). (c) I_D stability of microfluidic pH meter with/without photoresist protection layer on the AgCl/Ag p-RE at pH 6.5, 0.1 M KCl under a 10 µL/min flow rate. (d) Comparison of the influence of flow rate on the I_D of SiNRFETs in 0.03 M KCl between the measurements with an on-chip p-RE and with a commercial RE at the microfluidic outlet.

To verify this hypothesis, we repeated the drift measurements of the SiNRFET under an AC pulse gate bias applied via the AgCl/Ag p-RE: a positive pulse (1.3 V) is applied for 8 seconds, during which I_D is measured. This was followed by a 12-second negative gate pulse (-0.5 V), to release the interstitial hydrogen embedded in the HfO_2 layer back into the liquid. Fig. 4(c) shows that −0.5 V bias in the AC gate pulses effectively minimizes the I_D drift. The ΔV_{th} drift was reduced from about 10 mV/hour under constant gate bias to 1 mV/hour under the AC gate bias condition (see Fig. 4(d)). Once the negative pulse voltage is sufficient to desorb interstitial hydrogens from the HfO_2 layer, further increasing the negative pulse would not give additional benefit, as also evidenced in Fig. 4(d). Excessively high negative pulses may also cause AgCl decomposition. Our results show that using AC gate bias could be a very promising approach to minimize the signal drift in ISFET sensors.

3.4. Monitor bacterial metabolism using the microfluidic pH meter

To showcase the applicability of the integrated microfluidic pH meter, we used it to monitor the metabolism of *E. coli* in an LB medium with 1 wt.% glucose. Our measurements combined the microscale Ag/AgCl p-RE, the SiNRFET-microfluidics integration, and the AC pulse gate bias technique into a cohesive sensing platform, which enabled stable, real-time tracking of pH changes induced by bacterial metabolic activity using microliter-level samples.

The metabolism monitoring was conducted according to the following protocol. The microfluidic pH meter was placed on a holder that maintains temperature at 37 °C and connected to the readout instruments via a probe card. *E. coli* samples with different initial cell densities were prepared according to the description in Section 2.5. Then, each *E. coli* sample was injected into the microchannel of a microfluidic pH meter using a syringe pump. After sample loading, the surface of the microfluidic pH meter was covered by FC-70 oil to prevent liquid evaporation during the measurement. Additional control experiments in Fig. S6 demonstrated that the use of FC-70 oil did not affect the metabolic behavior of *E. coli* during on-chip culture. An AC pulse gate bias was applied via the AgCl/Ag p-RE: a positive 1.3 V pulse is applied for 10 seconds, during which I_D is measured. This was followed by a 10-second −0.5 V gate pulse, to minimize the SiNRFET drift during long-term pH monitoring. The acidification of the culture media induced by bacterial metabolism was directly measured as the threshold voltage shift (ΔV_{th}) of the SiNRFET during bacterial culturing.

Fig. 5(a) shows the pH changes of the culture medium over time during the on-chip culture of *E. coli* samples with different initial concentrations. In the presence of glucose, the metabolic products of *E. coli* acidify the culture media. Once the concentration of metabolic products exceeds a threshold, ΔV_{th} will increase until the pH of the culture medium reaches around pH 5. We define the onset time (t_{on}) as the time point where ΔV_{th} exceeded 10 mV, corresponding to significant acidification of the medium beyond the baseline drift (10 mV) observed in negative controls. The time point when ΔV_{th} remained stable within ± 10 mV over 30 min is defined as the time to steady state (t_{ss}), indicating that bacterial metabolism is inhibited by the acid environment. Fig. 5(b) shows the t_{on} and t_{ss} vs. initial bacterial concentration N_0. Within the investigated range of initial concentrations, both t_{on} and t_{ss} exhibit linear correlations with N_0. These t_{on} vs. N_0, and t_{ss} vs. N_0 curves can serve as calibration curves for determining the viable bacterial

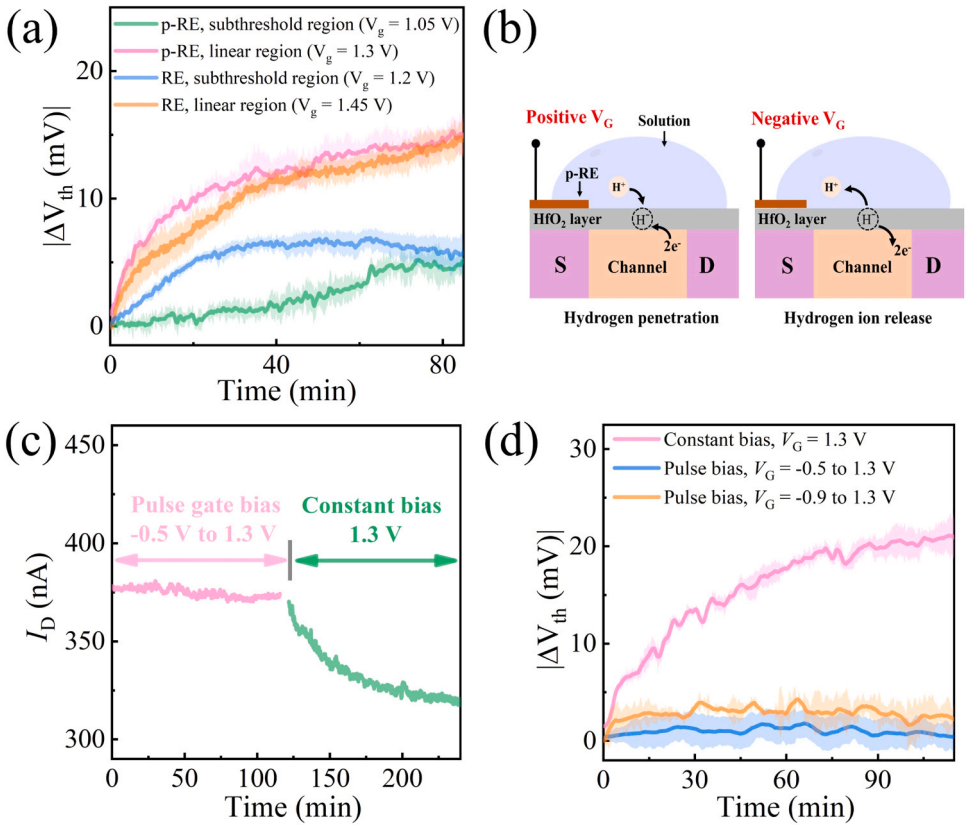

Fig. 4. Drift of SiNRFETs in 0.1 M KCl solution at pH 6.5, 20 °C, and static mode. (a) Threshold voltage drift of the SiNWFETs at constant gate bias. The light-shaded areas depict the standard deviations calculated from 3 SiNWFETs in the same test round. (b) Schematic illustrations of hydrogen ion penetration into the HfO_2 sensing layer under a positive gate bias (left), and hydrogen ion release from the HfO_2 sensing layer under a negative gate bias (right). (c) I_D drift of a SiNRFET first under AC pulse gate bias, then switches to constant gate bias. The gate bias is applied via the AgCl/Ag p-RE. (d) The threshold voltage drift of SiNRFET under different gate bias modes, using the AgCl/Ag p-RE.

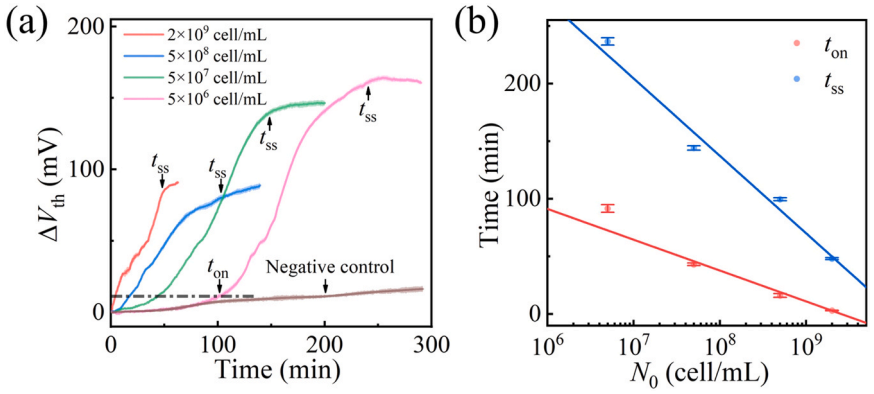

Fig. 5. (a) ΔV_{th} vs. time curves measured for *E. coli* on-chip culture at 37 °C with initial concentration N_0 of 2×10^9,5×10^8, 5×10^7, 5×10^6 cell/mL, using the microfluidic pH meter. The negative control is the LB solution without any *E. coli*. cell. Each curve was obtained by averaging the results measured by four SiNRFETs. The shaded areas along the solid lines depict the standard deviations calculated from 4 SiNRFET sensors and demonstrate a typical 1 mV standard deviation. (b) The onset time (t_{on}) and the time to steady state (t_{ss}) vs. the initial *E. coli* density N_0. The error bar depicts the standard deviation calculated from four SiNRFETs.

concentration in unknown samples, which is a key parameter to judge their clinical relevance. Additionally, the microfluidic pH meter requires only a μL amount of sample. This demonstration highlights the potential of the integrated system for on-chip analysis of cell samples, including quantifying cell density and real-time monitoring of cellular metabolic responses to various stimuli, such as drug treatments.

4. Conclusion

This study demonstrated the integration of on-chip microscale AgCl/Ag p-REs with SiNRFETs into a microfluidic pH meter. The integration addresses key challenges of ISFETs in microfluidic applications, including reference electrode miniaturization, streaming potential minimization, and ISFET signal drift. Protecting the p-REs with a photoresist layer effectively prevents the failure of p-REs during the sensing tests. The integrated microscale AgCl/Ag p-REs exhibited fast

stabilization and good long-term stability. Furthermore, the microscale distance between the p-REs and the SiNRFETs in the microfluidic system minimized the impacts from streaming potential to the sensing signal under varying flow conditions. The microfluidic pH meter could operate in static and flow modes, both with a close-to-Nernstian response. In addition, we demonstrated that applying an AC pulse gate bias could effectively reduce signal drift in the ISFET sensors caused by ion penetration into the pH-sensing layer, enhancing the system's reliability for real-time, long-term monitoring. The integrated microfluidic pH meter was finally used to real-time monitor the metabolic activity of bacteria within the microchannel, which highlights the potential of the integrated system for on-chip analysis of cell samples, including quantifying cell density and real-time monitoring of cellular metabolic responses to various stimuli, such as drug treatments [24]. Future research could focus on integrating ISFET sensors with advanced microfluidics to facilitate direct processing and analysis of clinical samples on-chip, even metabolic analysis at the single-cell level.

CRediT authorship contribution statement

Zheqiang Xu: Writing – original draft, Visualization, Methodology, Investigation, Data curation, Conceptualization. **Yingtao Yu:** Writing – review & editing, Methodology. **Paul Solomon:** Writing – review & editing, Methodology, Investigation, Conceptualization. **Zhen Zhang:** Writing – review & editing, Supervision, Resources, Funding acquisition, Conceptualization.

Declaration of Competing Interest

There are no conflicts of interest to declare.

Acknowledgments

This work was supported in part by the Swedish Research Council under Grant VR 2019–04690, in part by the Swedish Strategic Research Foundation under Grant SSF FFL15–0174, in part by the Wallenberg Academy Fellow Program under Grant KAW 2020–0190, and in part by the Stiftelsen Olle Engkvist under Postdoc grant 214–0322. The device fabrication was done in the Ångström Microstructure Laboratory (MSL), Uppsala University, and the technical staff of MSL are acknowledged for their process support. The bacterial strains used in this study were acquired from Koskiniemi-Lab, Department of Cell and Molecular Biology, Uppsala University. Sanna Koskiniemi and Victoria Nolan are acknowledged for their support.

Appendix A. Supporting information

Supplementary data associated with this article can be found in the online version at doi:10.1016/j.snb.2025.138000.

Data availability

Data will be made available on request.

References

[1] V. Iyer, D.A. Issadore, F. Aflatouni, The next generation of hybrid microfluidic/integrated circuit chips: recent and upcoming advances in high-speed, high-throughput, and multifunctional lab-on-IC systems, Lab Chip 23 (2023) 2553–2576, https://doi.org/10.1039/d2lc01163h.
[2] T. Lehnert, M.A.M. Gijs, Microfluidic systems for infectious disease diagnostics, Lab Chip 24 (2024) 1441–1493, https://doi.org/10.1039/d4lc00117f.
[3] K. Zhang, S. Qin, S. Wu, Y. Liang, J. Li, Microfluidic systems for rapid antibiotic susceptibility tests (ASTs) at the single-cell level, Chem. Sci. 11 (2020) 6352–6361, https://doi.org/10.1039/d0sc01353f.
[4] N. Jo, B. Kim, S.M. Lee, J. Oh, I.H. Park, K. Jin Lim, J.S. Shin, K.H. Yoo, Aptamer-functionalized capacitance sensors for real-time monitoring of bacterial growth and antibiotic susceptibility, Biosens. Bioelectron. 102 (2018) 164–170, https://doi.org/10.1016/j.bios.2017.11.010.
[5] E. Garcia-Cordero, F. Bellando, J. Zhang, F. Wildhaber, J. Longo, H. Guerin, A. M. Ionescu, Three-dimensional integrated ultra-low-volume passive microfluidics with ion-sensitive field-effect transistors for multiparameter wearable sweat analyzers, ACS Nano 12 (2018) 12646–12656, https://doi.org/10.1021/acsnano.8b07413.
[6] J.M. Rothberg, W. Hinz, T.M. Rearick, J. Schultz, W. Mileski, M. Davey, J. H. Leamon, K. Johnson, M.J. Milgrew, M. Edwards, J. Hoon, J.F. Simons, D. Marran, J.W. Myers, J.F. Davidson, A. Branting, J.R. Nobile, B.P. Puc, D. Light, T.A. Clark, M. Huber, J.T. Branciforte, I.B. Stoner, S.E. Cawley, M. Lyons, Y. Fu, N. Homer, M. Sedova, X. Miao, B. Reed, J. Sabina, E. Feierstein, M. Schorn, M. Alanjary, E. Dimalanta, D. Dressman, R. Kasinskas, T. Sokolsky, J.A. Fidanza, E. Namsaraev, K.J. McKernan, A. Williams, G.T. Roth, J. Bustillo, An integrated semiconductor device enabling non-optical genome sequencing, Nature 475 (2011) 348–352, https://doi.org/10.1038/nature10242.
[7] M. Douthwaite, N. Moser, P. Georgiou, CMOS ISFET arrays for integrated electrochemical sensing and imaging applications: a tutorial, IEEE Sens. J. 21 (2021) 22155–22169, https://doi.org/10.1109/jsen.2021.3094206.
[8] M. Shojaei Baghini, A. Vilouras, R. Dahiya, Ultra-thin chips with ISFET array for continuous monitoring of body fluids Ph, IEEE Trans. Biomed. Circuits Syst. 15 (2021) 1174–1185, https://doi.org/10.1109/TBCAS.2022.3141553.
[9] M. Duan, X. Zhong, X. Zhao, O.M. El-Agnaf, Y.K. Lee, A. Bermak, An optical and temperature assisted CMOS ISFET sensor array for robust E. Coli detection, IEEE Trans. Biomed. Circuits Syst. 15 (2021) 497–508, https://doi.org/10.1109/TBCAS.2021.3084540.
[10] C. Duarte-Guevara, V. Swaminathan, B. Reddy, C.-H. Wen, Y.-J. Huang, J.-C. Huang, Y.-S. Liu, R. Bashir, Characterization of a 1024 × 1024 DG-BioFET platform, Sens. Actuators B: Chem. 250 (2017) 100–110, https://doi.org/10.1016/j.snb.2017.04.107.
[11] X. Chen, Q. Hu, S. Chen, N.L. Netzer, Z. Wang, S.-L. Zhang, Z. Zhang, Multiplexed analysis of molecular and elemental ions using nanowire transistor sensors, Sens. Actuators B: Chem. 270 (2018) 89–96, https://doi.org/10.1016/j.snb.2018.05.018.
[12] Q. Hu, S. Chen, P. Solomon, Z. Zhang, Ion sensing with single charge resolution using sub–10-nm electrical double layer–gated silicon nanowire transistors, Sci. Adv. 7 (2021) eabj6711, https://doi.org/10.1126/sciadv.abj6711.
[13] Y. Kutovyi, H. Hlukhova, N. Boichuk, M. Menger, A. Offenhausser, S. Vitusevich, Amyloid-beta peptide detection via aptamer-functionalized nanowire sensors exploiting single-trap phenomena, Biosens. Bioelectron. 154 (2020) 112053, https://doi.org/10.1016/j.bios.2020.112053.
[14] G. Alexandrou, N. Moser, K.T. Mantikas, J. Rodriguez-Manzano, S. Ali, R. C. Coombes, J. Shaw, P. Georgiou, C. Toumazou, M. Kalofonou, Detection of multiple breast cancer ESR1 mutations on an ISFET based lab-on-chip platform, IEEE Trans. Biomed. Circ. S 15 (2021) 380–389, https://doi.org/10.1109/Tbcas.2021.3094464.
[15] P. Bergveld, Thirty years of ISFETOLOGY - what happened in the past 30 years and what may happen in the next 30 years, Sens. Actuators B-Chem. 88 (2003) 1–20, https://doi.org/10.1016/S0925-4005(02)00301-5.
[16] M.W. Shinwari, D. Zhitomirsky, I.A. Deen, P.R. Selvaganapathy, M.J. Deen, D. Landheer, Microfabricated reference electrodes and their biosensing applications, Sensors 10 (2010) 1679–1715, https://doi.org/10.3390/s100301679.
[17] F. Sassa, G.C. Biswas, H. Suzuki, Microfabricated electrochemical sensing devices, Lab Chip 20 (2020) 1358–1389, https://doi.org/10.1039/c9lc01112a.
[18] S. Søpstad, E.A. Johannessen, F. Seland, K. Imenes, Long-term stability of screen-printed pseudo-reference electrodes for electrochemical biosensors, Electrochim. Acta 287 (2018) 29–36, https://doi.org/10.1016/j.electacta.2018.08.045.
[19] Z. Zhao, H. Tu, E.G. Kim, B.F. Sloane, Y. Xu, A flexible Ag/AgCl micro reference electrode based on a parylene tube structure, Sens Actuators B Chem. 247 (2017) 92–97, https://doi.org/10.1016/j.snb.2017.02.135.
[20] Q. Li, W. Tang, Y. Su, Y. Huang, S. Peng, B. Zhuo, S. Qiu, L. Ding, Y. Li, X. Guo, Stable thin-film reference electrode on plastic substrate for all-solid-state ion-sensitive field-effect transistor sensing system, IEEE Electron Device Lett. 38 (2017) 1469–1472, https://doi.org/10.1109/led.2017.2732352.
[21] S. Papamatthaiou, U. Zupancic, C. Kalha, A. Regoutz, P. Estrela, D. Moschou, Ultra stable, inkjet-printed pseudo reference electrodes for lab-on-chip integrated electrochemical biosensors, Sci. Rep. 10 (2020) 17152, https://doi.org/10.1038/s41598-020-74340-1.
[22] B.K. Troudt, C.R. Rousseau, X.I.N. Dong, E.L. Anderson, P. Buhlmann, Recent progress in the development of improved reference electrodes for electrochemistry, Anal. Sci. 38 (2022) 71–83, https://doi.org/10.2116/analsci.21SAR11.
[23] P.-Y. Kuo, T.-H. Wang, M.-T. Hsu, C.-H. Liao, Design and fabrication of PDMS microfluidic device combined with urea biosensor for dynamic and static measurements, IEEE J. Electron Devices Soc. 11 (2023) 337–346, https://doi.org/10.1109/jeds.2023.3283533.
[24] X. Xu, S. Chen, Y. Yu, P. Virtanen, J. Wu, Q. Hu, S. Koskiniemi, Z. Zhang, All-electrical antibiotic susceptibility testing within 30 min using silicon nano transistors, Sens. Actuators B: Chem. 357 (2022), https://doi.org/10.1016/j.snb.2022.131458.
[25] R.C. Dawkins, D. Wen, J.N. Hart, M. Vepsäläinen, A screen-printed Ag/AgCl reference electrode with long-term stability for electroanalytical applications, Electrochim. Acta 393 (2021), https://doi.org/10.1016/j.electacta.2021.139043.
[26] H. Zhang, R. Chuai, X. Li, B. Zhang, Design, preparation and performance study of on-chip flow-through amperometric sensors with an integrated Ag/AgCl reference electrode, Micromachines 9 (2018), https://doi.org/10.3390/mi9030114.
[27] J. Zhou, K. Ren, Y. Zheng, J. Su, Y. Zhao, D. Ryan, H. Wu, Fabrication of a microfluidic Ag/AgCl reference electrode and its application for portable and

disposable electrochemical microchips, Electrophoresis 31 (2010) 3083–3089, https://doi.org/10.1002/elps.201000113.
[28] R. Vinoth, T. Nakagawa, J. Mathiyarasu, A.M.V. Mohan, Fully printed wearable microfluidic devices for high-throughput sweat sampling and multiplexed electrochemical analysis, ACS Sens. 6 (2021) 1174–1186, https://doi.org/10.1021/acssensors.0c02446.
[29] S. Wang, M. Rovira, S. Demuru, C. Lafaye, J. Kim, B.P. Kunnel, C. Besson, C. Fernandez-Sanchez, F. Serra-Graells, J.M. Margarit-Taule, J. Aymerich, J. Cuenca, I. Kiselev, V. Gremeaux, M. Saubade, C. Jimenez-Jorquera, D. Briand, S. C. Liu, Multisensing wearables for real-time monitoring of sweat electrolyte biomarkers during exercise and analysis on their correlation with core body temperature, IEEE Trans. Biomed. Circuits Syst. 17 (2023) 808–817, https://doi.org/10.1109/TBCAS.2023.3286528.
[30] Y. Zhang, Y. Zhu, S. Zheng, L. Zhang, X. Shi, J. He, X. Chou, Z.-S. Wu, Ink formulation, scalable applications and challenging perspectives of screen printing for emerging printed microelectronics, J. Energy Chem. 63 (2021) 498–513, https://doi.org/10.1016/j.jechem.2021.08.011.
[31] A. Simonis, M. Dawgul, H. Lüth, M.J. Schöning, Miniaturised reference electrodes for field-effect sensors compatible to silicon chip technology, Electrochim. Acta 51 (2005) 930–937, https://doi.org/10.1016/j.electacta.2005.04.063.
[32] Y. Cui, M.A. Moreira, K.E. Whalen, L. Barbe, Q. Shi, K. Koren, M. Tenje, L. Behrendt, SlipO(2)Chip - single-cell respiration under tuneable environments, Lab Chip 24 (2024) 4786–4797, https://doi.org/10.1039/d4lc00420e.
[33] B. Lin, Z. Guo, Z. Geng, S. Jakaratanopas, B. Han, P. Liu, A scalable microfluidic chamber array for sample-loss-free and bubble-proof sample compartmentalization by simple pipetting, Lab Chip 20 (2020) 2981–2989, https://doi.org/10.1039/d0lc00348d.
[34] J. Avesar, D. Rosenfeld, M. Truman-Rosentsvit, T. Ben-Arye, Y. Geffen, M. Bercovici, S. Levenberg, Rapid phenotypic antimicrobial susceptibility testing using nanoliter arrays, Proc. Natl. Acad. Sci. USA 114 (2017) E5787–E5795, https://doi.org/10.1073/pnas.1703736114.
[35] M. Azizi, M. Zaferani, B. Dogan, S. Zhang, K.W. Simpson, A. Abbaspourrad, Nanoliter-sized microchamber/microarray microfluidic platform for antibiotic susceptibility testing, Anal. Chem. 90 (2018) 14137–14144, https://doi.org/10.1021/acs.analchem.8b03817.
[36] D. Hummer, F. Kurth, N. Naredi-Rainer, P.S. Dittrich, Single cells in confined volumes: microchambers and microdroplets, Lab Chip 16 (2016) 447–458, https://doi.org/10.1039/c5lc01314c.
[37] O. Baltekin, A. Boucharin, E. Tano, D.I. Andersson, J. Elf, Antibiotic susceptibility testing in less than 30 min using direct single-cell imaging, Proc. Natl. Acad. Sci. USA 114 (2017) 9170–9175, https://doi.org/10.1073/pnas.1708558114.
[38] A.M. Kaushik, K. Hsieh, L. Chen, D.J. Shin, J.C. Liao, T.H. Wang, Accelerating bacterial growth detection and antimicrobial susceptibility assessment in integrated picoliter droplet platform, Biosens. Bioelectron. 97 (2017) 260–266, https://doi.org/10.1016/j.bios.2017.06.006.
[39] Y. Song, J. Yin, W.E. Huang, B. Li, H. Yin, Emerging single-cell microfluidic technology for microbiology, Trends Anal. Chem. 170 (2024), https://doi.org/10.1016/j.trac.2023.117444.
[40] S.-C. Park, H.J. Jeong, M. Heo, J.H. Shin, J.-H. Ahn, Carbon nanotube-based ion-sensitive field-effect transistors with an on-chip reference electrode toward wearable sodium sensing, ACS Appl. Electron. Mater. 3 (2021) 2580–2588, https://doi.org/10.1021/acsaelm.1c00152.
[41] D. Welch, S. Shah, S. Ozev, J. Blain Christen, Experimental and simulated cycling of ISFET electric fields for drift reset, IEEE Electron Device Lett. 34 (2013) 456–458, https://doi.org/10.1109/led.2013.2240648.
[42] S. Jamasb, An analytical technique for counteracting drift in ion-selective field effect transistors (ISFETs), IEEE Sens. J. 4 (2004) 795–801, https://doi.org/10.1109/jsen.2004.833148.
[43] J. Liang, X. Jia, Y. HuMiniaturized and Integrated On-Chip Ag/AgCl Micro-electrodes for Chemical Detection. 2024 IEEE International Symposium on Circuits and Systems (ISCAS). 2024. pp. 1-5. https://doi.org/10.1109/iscas58744.2024.10558327..
[44] D. Lee, D. Jung, F. Jiang, G.V. Junek, J. Park, H. Liu, Y. Kong, A. Wang, Y. Kim, K. S. Choi, J. Wang, H. Wang, A multi-functional CMOS biosensor array with on-chip DEP-assisted sensing for rapid low-concentration analyte detection and close-loop particle manipulation with no external electrodes, IEEE Trans. Biomed. Circuits Syst. 17 (2023) 1214–1226, https://doi.org/10.1109/TBCAS.2023.3343068.
[45] C. Duarte-Guevara, V.V. Swaminathan, M. Burgess, B. Reddy Jr., E. Salm, Y.S. Liu, J. Rodriguez-Lopez, R. Bashir, On-chip metal/polypyrrole quasi-reference electrodes for robust ISFET operation, Analyst 140 (2015) 3630–3641, https://doi.org/10.1039/c5an00085h.
[46] K. Dawson, A. Wahl, S. Barry, C. Barrett, N. Sassiat, A.J. Quinn, A. O'Riordan, Fully integrated on-chip nano-electrochemical devices for electroanalytical applications, Electrochim. Acta 115 (2014) 239–246, https://doi.org/10.1016/j.electacta.2013.10.144.
[47] Z. Xu, S. Chen, Q. Hu, S.-L. Zhang, Z. Zhang, A nanoribbon-based ion-gated lateral bipolar amplifier for ion sensing, IEEE Trans. Electron Devices 71 (2024) 4362–4367, https://doi.org/10.1109/ted.2024.3400926.
[48] K. Stevenson, A.F. McVey, I.B.N. Clark, P.S. Swain, T. Pilizota, General calibration of microbial growth in microplate readers, Sci. Rep. 6 (2016) 38828, https://doi.org/10.1038/srep38828.
[49] G. Sezonov, D. Joseleau-Petit, R. D'Ari. Escherichia coli physiology in Luria-Bertani broth, J. Bacteriol. 189 (2007) 8746–8749, https://doi.org/10.1128/JB.01368-07.
[50] Y. Qin, A.U. Alam, M.M.R. Howlader, N.X. Hu, M.J. Deen, inkjet printing of a highly loaded palladium ink for integrated, low-cost pH sensors, Adv. Funct. Mater. 26 (2016) 4923–4933, https://doi.org/10.1002/adfm.201600657.
[51] H.-R. Lim, N. Hillman, Y.-T. Kwon, Y.-S. Kim, Y.-H. Choa, W.-H. Yeo, Ultrathin, long-term stable, solid-state reference electrode enabled by enhanced interfacial adhesion and conformal coating of AgCl, Sens. Actuators B: Chem. 309 (2020), https://doi.org/10.1016/j.snb.2020.127761.
[52] M. Parmeggiani, A. Dev, P. Björk, J. Linnros, Electrokinetic-assisted gating in a microfluidic integrated Si nanoribbon ion sensor for enhanced sensitivity, Sens. Actuators B: Chem. 262 (2018) 974–981, https://doi.org/10.1016/j.snb.2018.02.017.
[53] J. Lee, M. Wipf, L. Mu, C. Adams, J. Hannant, M.A. Reed, Metal-coated microfluidic channels: An approach to eliminate streaming potential effects in nano biosensors, Biosens. Bioelectron. 87 (2017) 447–452, https://doi.org/10.1016/j.bios.2016.08.065.
[54] L. Manjakkal, D. Szwagierczak, R. Dahiya, Metal oxides based electrochemical pH sensors: current progress and future perspectives, Prog. Mater. Sci. 109 (2020), https://doi.org/10.1016/j.pmatsci.2019.100635.
[55] D.W. Kwon, S. Kim, R. Lee, H.-S. Mo, D.H. Kim, B.-G. Park, Macro modeling of ion sensitive field effect transistor with current drift, Sens. Actuators B: Chem. 249 (2017) 564–570, https://doi.org/10.1016/j.snb.2017.03.110.
[56] M. Houssa, V.V. Afanas'ev, A. Stesmans, M.M. Heyns, Variation in the fixed charge density of SiOx/ZrO2 gate dielectric stacks during postdeposition oxidation, Appl. Phys. Lett. 77 (2000) 1885–1887, https://doi.org/10.1063/1.1310635.
[57] S.J. Lee, C.H. Choi, A. Kamath, R. Clark, D.L. Kwong, Characterization and reliability of dual high-k gate dielectric stack (poly-Si-HfO2-SiO2) prepared by in situ RTCVD process for system-on-chip applications, IEEE Electron Device Lett. 24 (2003) 105–107, https://doi.org/10.1109/led.2002.807712.
[58] J.L. Lyons, A. Janotti, C.G. Van de Walle, The role of oxygen-related defects and hydrogen impurities in HfO2 and ZrO2, Microelectron. Eng. 88 (2011) 1452–1456, https://doi.org/10.1016/j.mee.2011.03.099.
[59] J. Kang, E.-C. Lee, K.J. Chang, Y.-G. Jin, H-related defect complexes in HfO2: a model for positive fixed charge defects, Appl. Phys. Lett. 84 (2004) 3894–3896, https://doi.org/10.1063/1.1738946.

Zheqiang Xu received his B. Eng. Degree in Material Science and Engineering from Harbin Institute of Technology, China in 2017. And received his M.Sc. degree in Material Science and Engineering from University of Science and Technology of China in 2020. He is currently pursuing his Ph.D. in Electrical Engineering at the division of solid-state electronics at Uppsala University in Uppsala, Sweden. His research interests include nanoscale semiconductor devices, microfluidics, and bioelectronics.

Yingtao Yu is currently a postdoctoral researcher at Uppsala University, Sweden. He received his B.S. degree (2018) from University of Science and Technology of China. He received his Ph.D. degree (2023) in Electrical Engineering from Uppsala University, Sweden. His research interests include nano-devices for sensing applications, piezoresistive NEMS, and biosensors.

Paul Michael Solomon received his Ph.D. from Technion, Haifa, Israel, in 1974. Since 1975, he has been a Research Staff Member at the T. J. Watson Research Center, IBM, Yorktown Heights, NY, working on high-speed semiconductor devices.

Zhen Zhang is a professor of solid-state electronics at Uppsala University in Uppsala, Sweden. He received a Ph.D. degree in the Department of Microelectronics and Information Technology from Royal Institute of Technology (KTH) of Sweden in 2008. He worked as a research staff member at IBM T. J. Watson research center at Yorktown Heights, New York from 2008 to 2013, and joined Uppsala University in 2013. His research interest covers semiconductor-based electronic sensors, nanoscale semiconductor devices, and bioelectronics.